Seismic analysis of a tall metal wind turbine support tower with realistic geometric imperfections

Adam Jan Sadowski[1], Alfredo Camara[2], Christian Málaga-Chuquitaype[1], Kaoshan Dai[3]

Abstract

The global growth in wind energy suggests that wind farms will increasingly be deployed in seismically active regions, with large arrays of similarly-designed structures potentially at risk of simultaneous failure under a major earthquake. Wind turbine support towers are often constructed as thin-walled metal shell structures, well-known for their imperfection sensitivity, and are susceptible to sudden buckling failure under compressive axial loading.

This study presents a comprehensive analysis of the seismic response of a 1.5 MW wind turbine steel support tower modelled as a near-cylindrical shell structure with realistic axisymmetric weld depression imperfections. A selection of twenty representative earthquake ground motion records, ten 'near-fault' and ten 'far-field', was applied and the aggregate seismic response explored using lateral drifts and total plastic energy dissipation during the earthquake as structural demand parameters.

The tower was found to exhibit high stiffness, though global collapse may occur soon after the elastic limit is exceeded through the development of a highly unstable plastic hinge under seismic excitations. Realistic imperfections were found to have a significant effect on the intensities of ground accelerations at which damage initiates and on the failure location, but only a small effect on the vibration properties and the response prior to damage. Including vertical accelerations similarly had a limited effect on the elastic response, but potentially shifts the location of the plastic hinge to a more slender and therefore weaker part of the tower. The aggregate response was found to be significantly more damaging under near-fault earthquakes with pulse-like effects and large vertical accelerations than far-field earthquakes without these aspects.

Keywords

Thin metal shell structure, imperfection sensitivity, seismic response, multiple stripe analysis, near-fault ground motions, vertical ground acceleration.

[1]Department of Civil and Environmental Engineering, Imperial College London, UK
[2]Department of Civil Engineering at City, University of London, UK
[3]State Key Laboratory of Disaster Reduction in Civil Engineering, Tongji University, Shanghai, China

Please Cite as:
Sadowski AJ, Camara A, Málaga-Chuquitaype C, Dai K., 2017, Seismic analysis of a tall metal wind turbine support tower with realistic geometric imperfections, *Earthquake Engineering and Structural Dynamics*, **46**: 201-219. ISSN:0098-8847

1. Introduction

It is increasingly recognised that future energy needs must draw on renewable fuel sources in order to reduce CO_2 emissions and combat climate change [1,2], with wind energy currently representing the fastest growth area of all renewables. As of 2013, wind energy supplied 3% of the world's electricity supply [2], a figure that is set to grow in line with economic development in energy-hungry emerging markets, and as the technology develops and costs fall. Earthquake-prone China in particular is a world leader, with 31% of the global wind power capacity [1].

The growth in global wind energy suggests that wind farms will increasingly be constructed in seismically active regions, and entire arrays of similarly-designed structures may become at risk of failing simultaneously under an extreme seismic event [3,4]. It is therefore important to understand the behaviour of these structures under realistic assessments of seismic loading. There is a dearth of information in this regard, with studies in the field focusing mainly on assessing fatigue in the turbine machinery [5,6] and on blade design [7]. The static or dynamic response of the support tower itself has been considered mostly in the context of wind loading [8,9], with seismic loading usually deemed to be only of secondary importance and treated according to simple codified provisions [10,11].

Only very few published studies appear to have considered the nonlinear dynamic response of a wind turbine support tower in the time domain [3,12,13]. Nuta *et al.* [3] were possibly the first to perform an incremental dynamic analysis, investigating a 80 m tall 1.65 MW wind turbine steel tower with diameter to thickness (d/t) ratios ranging from 105 to 278 using suites of earthquake records representing North American seismic activity, including Los Angeles and Western Canada. While it was found that the tower performed well under each record, a consequence of its fundamental vibration period being significantly longer than the dominant period of most earthquakes, they illustrated that collapse can occur suddenly if the elastic limit is exceeded at higher ground accelerations.

More recently, Stamatopoulos [13] performed both a response spectrum and a single time-history analysis on a 54 m tall 'perfect' hollow steel tower with d/t ratios ranging from 51 to 134 and a foundation modelled using nonlinear springs. A codified design spectrum was used, amongst others, amplified by 25% to account for 'near-fault' conditions. It was found that the time-history analysis predicted almost 50% higher values of base shear and overturning moment compared with a response spectrum analysis. This effect was attributed to a time-history analysis being able to correctly capture shear waves travelling up the structure by the activation of higher modes, illustrating the importance of using a more sophisticated analysis to obtain a safe and realistic assessment of the seismic response of such structures. A complete recent literature review of the topic by Katsanos *et al.* [14] concluded that the effects of near-fault records on wind turbines require further investigation.

2. Scope of the study

Steel towers supporting wind turbine machinery typically have d/t ratios ranging from 50 to more than 300, classifying them most often as 'slender' hollow sections under uniform compression and flexure according to EN 1993-1-1 [15], AISC 360-10 [16] and other standards. The support towers are in fact thin-walled near-cylindrical shells, particularly susceptible to local buckling under the increased axial membrane

compression that often accompanies seismic loading. This additional compression arises above all from global cantilever action under horizontal ground accelerations, but also directly due to vertical ground accelerations.

The detrimental effect of geometric imperfections on the behaviour of thin cylindrical shells under fundamental static loads, and axial compression in particular, is well known in the shells literature [17-19]. However, studies within earthquake engineering that explicitly account for imperfections in shell structures are rare. Known to the authors is only the study of Guo *et al.* [20] who performed a geometrically and materially nonlinear pushover analysis on an example 53 m high steel wind turbine tower with tapering *d/t* ratio ranging from 121 to 184. They introduced a single localised 'dent' imperfection of up to 5% of the diameter, intended to simulate the effects of an accidental impact, in the upper segments of the tower. However, this choice of imperfection form did not show any significant decrease in the predicted buckling strength, possibly because the most critical region for buckling under their assumed load distribution was at the base of the tower away from the position of the imperfection. This is not thought to be a representative result, and it is more likely that imperfections will be at least as deleterious to the seismic response of hollow metal wind turbine towers as to the static response [4].

The authors are not aware of any comprehensive study of the effect of realistic geometric imperfections, attributable to a systematic manufacturing process, on the general seismic response of a hollow steel wind turbine support tower, as is undertaken in this paper. Initial studies, including modal analysis and model optimisation, are followed by two multiple stripe analyses (MSAs) using a representative selection of twenty earthquake ground motion accelerograms, comprised of ten 'near-fault' records with distinct velocity pulses and ten 'far-field' records without. The MSAs are illustrated using lateral drift and plastic energy dissipation demand measures. The first MSA considers the influence of increasing imperfection amplitudes on the tower's nonlinear seismic response under selected individual records, both with and without the vertical acceleration component. The second MSA investigates the aggregate seismic response of the perfect and most imperfect structures under the full set of twenty earthquake records and two levels of structural damping.

3. Modelling of an imperfect wind turbine support tower as a shell

The structure considered in this study is a 61 m hollow tubular steel tower supporting a 1.5MW capacity three-bladed horizontal-axis NORDEX S70/1500 wind turbine. It was designed according to Class IIa in IEC 61400-1 [21] with a 10-minute reference wind speed of 42.5 m/s at hub height and a turbulence intensity of 0.16. Towers like this have been constructed in Chinese wind farms near Shanghai since the early 2000s, and are representative of many such structures currently in operation in the world today. The structural design was performed commercially by a third party according to DIN 18800-1 [22] with no explicit seismic provisions. The outer diameter d_o of the tapering tower varied from 4035 mm at the base to 2955 mm at the top, while the shell wall thickness t varied from 25 mm at the base to a minimum of 10 mm near the top. The outer diameter to wall thickness (d_0/t) ratio varies from a minimum of ~161 at the base to a maximum of ~375 in the upper regions of the tower (Fig. 1), indicating a particularly slender near-cylindrical shell structure. The mass of the support tower was approximately 91 tonnes.

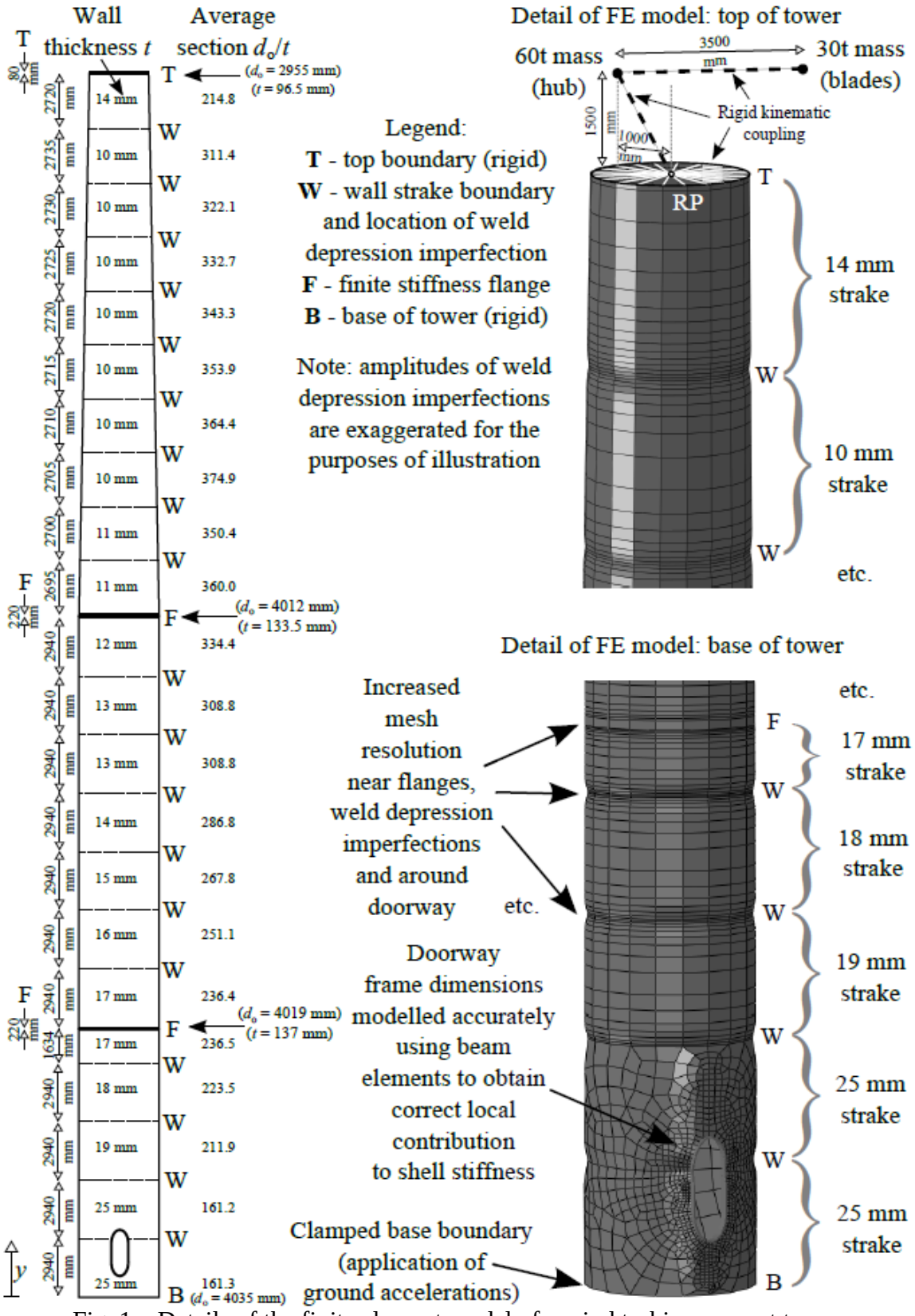

Fig. 1 – Details of the finite element model of a wind turbine support tower

The structure was modelled with finite elements using the commercial ABAQUS 6.14-2 [23] code, with relevant details shown in Fig. 1. Only those design features deemed necessary to accurately capture the global seismic response were included. The shell wall was modelled using a mesh of linear reduced-integration finite-strain S4R general

purpose shell elements, suitable for both static and dynamic analyses including extensive plasticity, validated using a series of careful preliminary mesh convergence studies (an example of which is shown in Fig. 2). Care was taken to ensure that the chosen mesh predicted the same plastic hinge location as higher resolution meshes, a mechanism of failure that plays an important role in what follows.

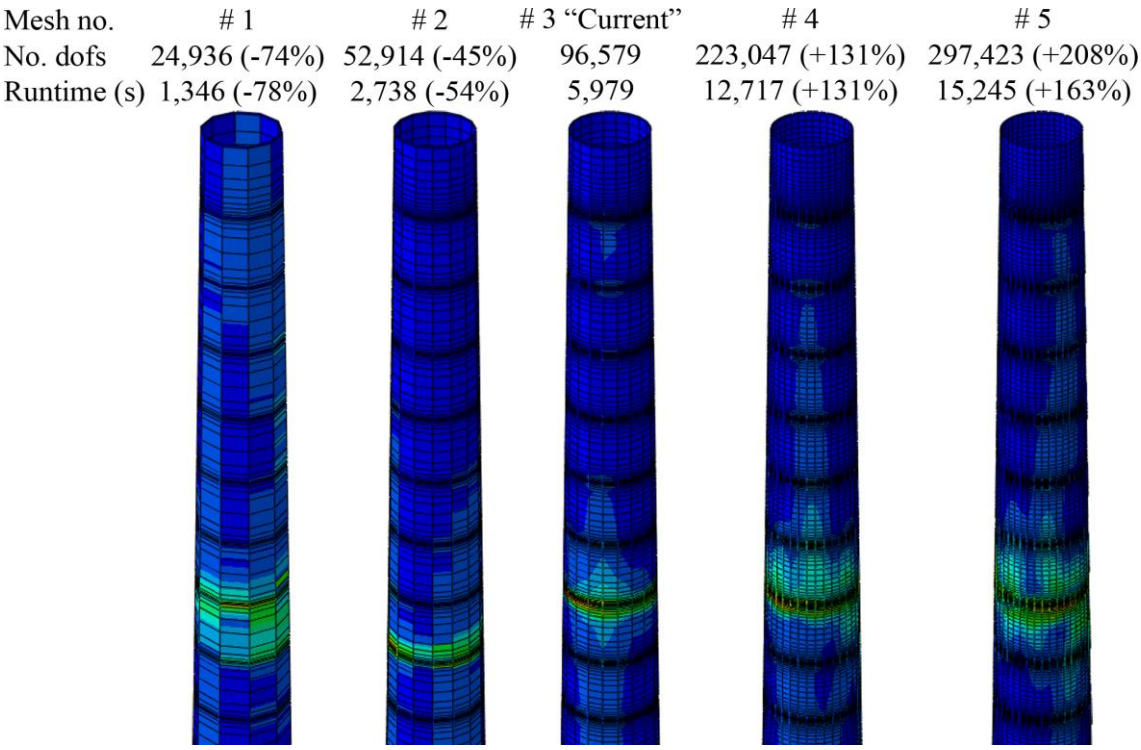

Fig. 2 – Illustration of mesh convergence study: five different meshes under a 10-second scaled nonlinear time-history seismic record (Pacoima Dam), with dof and runtime costs relative to final 'current' mesh, and sensitivity to plastic hinge location

A simple ideal elastic-plastic material law was applied with a yield stress of 355 MPa, Poisson's ratio of 0.3, an elastic modulus of 200 GPa and a density of 7850 kg/m^3, representing a generic S355 mild steel grade as assumed in design. An initial sensitivity study investigated the effects of post-yield linear strain hardening (up to 2% of the elastic modulus) and found that only a very small amount of strain hardening (0.1%) was sufficient to accurately illustrate the qualitative phenomena presented in this paper and enhance numerical stability. Additionally, and for reasons that will be explained in what follows, a simple 'frictionless' tangential and 'hard' normal self-contact rule was permitted.

The reinforced-concrete tower foundation was not modelled explicitly but simulated as a rigid clamped circular boundary at the base nodes ('B' in Fig. 1). Recent studies suggest that foundations built on soft soil potentially increase the vibration fundamental periods and exacerbate the seismic response of such tall yet rigid structures [4,13,24], though others suggest that the relative flexibility of the shell wall near the base support and the tower's overall low weight lead to only a modest transmission of energy from the foundation during an earthquake [25]. As this study focuses specifically on the sensitivity of the seismic response of the tower to realistic manufacturing defects, it was felt that an assessment of seismic risk of a wind turbine due to soil-structure interaction lies outside the scope.

The top of the tower ('T' in Fig. 1) must in practice be sufficiently stiff to support the heavy turbine machinery. The top boundary was therefore modelled assuming a rigid body kinematic coupling between the top edge shell nodes and a reference point on the centroid of the tower, maintaining a circular cross-section. The machinery was modelled as two distinct lumped masses of 60 tonnes and 30 tonnes offset at 3.5 m representing the hub and blades respectively, also connected to each other and to the top boundary with a rigid body kinematic coupling. An initial sensitivity analysis found the influence of the rotary inertia of the blades on the initial vibration modes of the structure to be negligible (relative difference less than 0.005%). The flexibility of the blades is also ignored in the present work, an assumption that is in agreement with other studies of this nature [3]. Similarly, the orientation of the nacelle had a negligible effect on the fundamental frequencies and response history of the structure (average coefficient of variation less than 0.025% for the first 400 vibration modes across 72 different orientations).

The design included two internal platforms at a height of approximately 13 and 34 m. Although the contribution of the slender platforms to the global mass is negligible, they are supported on stiffening rings or flanges ('F' in Fig. 1) whose increased local thickness helps maintain circularity of the tower cross-section and contributes significantly to the global bending stiffness. For simplicity and computational efficiency, these flanges were modelled as another shell segment endowed with a greater wall thickness to account for the additional mass and stiffness. An accurately-rendered elliptical cut-out representing the doorway was included in the lowest two wall segments, its reinforcing 40 mm thick frame modelled with beam elements to obtain a realistic assessment of its contribution to the local stiffness.

In contrast to structures such as buildings or bridges, the code-prescribed structural damping ratio of 5% (e.g. EN 1998-1 [26]; EN 1998-6 [27]) for a slender wind turbine support tower is debatable. While it is reported [3,12] that a damping ratio of 5% is a reasonable assumption for a tower with an operating turbine, where the rotating blades contribute significantly to the aerodynamic damping, a 'parked' turbine offers no such contribution and the total damping for the tower may be as low as 0.5 – 1% [3,4,10,13,21,28,29] potentially leading to a significant amplification of the seismic load. The aerodynamic damping also depends on the direction of the wind with respect to the position of the blades. The constant damping ratios recommended in [30] for 1.5 MW wind turbines are considered in the full set of dynamic analyses, namely 1% damping to represent the 'parked' condition in all wind directions or operational conditions with side-to-side wind directions, and 5% damping to represent operational conditions with wind in the fore-aft direction.

A metal wind turbine support tower is typically constructed by welding together individual segments or 'strakes' of rolled sheet metal, a process common to other large-scale cylindrical shell structures such as silos, pressure vessels, liquid-storage tanks, pipelines and chimneys. The strake edges undergo a slight inward curl due to shrinking during post-weld cooling [31,32], leading to a well-defined geometric imperfection along the line of the weld. Its radial profile $w(y)$ may be modelled accurately using the Type 'A' axisymmetric weld depression of Rotter and Teng [31]:

$$w(y) = \delta_0 e^{-\pi|y-y_w|/\lambda}\left[\cos\left(\frac{\pi}{\lambda}|y-y_w|\right)+\sin\left(\frac{\pi}{\lambda}|y-y_w|\right)\right] \text{ where } \lambda = \frac{\pi\sqrt{rt}}{\sqrt[4]{3\left(1-\nu^2\right)}} \qquad (1)$$

In the above, δ_0 is the imperfection amplitude, r and t are the local shell mid-surface radius and wall thickness respectively, v is the Poisson ratio, y is the global axial coordinate with origin at the base of the tower and y_w is the vertical location of the centre of the weld depression. The parameter λ is the linear axial bending half-wavelength from classical shell bending theory [33] controlling the extent of the penetration of the depression into the shell, vanishing exponentially away from y_w.

The axisymmetric weld depression imperfection is well known in the shell buckling community as a realistic characterisation of unavoidable geometric deviations arising from a systematic manufacturing process. It has been shown to qualitatively reproduce geometric deviation profiles measured in full-scale surveys of completed cylindrical shell structures across a wide range of d/t ratios [34-36]. It has been widely implemented in numerous numerical studies to assess the imperfection sensitivity of cylindrical shells under static loading conditions of uniform axial compression [37-40], uniform global bending [41] and localised loading [42-44]. The consensus is that the weld depression is likely to be the most deleterious imperfection form possible for thin cylindrical shells under conditions of approximate uniform axial compression [19]. A detailed discussion of more classical 'eigenmode-affine' imperfections, which are commonly applied but difficult to justify on the basis of realism, may be found in [45].

The global bending cantilever response of the tower is carried as a circumferentially varying axial membrane action which, on the compressed side, causes stress conditions approaching uniform compression. Further, near-field earthquake in particular may also contain a significant vertical acceleration component that may introduce higher magnitudes of axial compression into the tower and potentially amplify the seismic damage, with geometric imperfections further exacerbating this effect. This is one of the hypotheses investigated in this paper.

The European Standard on Metal Shells EN 1993-1-6 [46] specifies imperfection amplitudes and tolerances during design and construction by prescribing one of three Fabrication Tolerance Quality (FTQ) Classes, defined in order of decreasing quality (increasing imperfection amplitude) as follows: A or 'Excellent', B or 'Very Good' and C or 'Normal'. The state-of-the-art special provisions for 'structural design by global numerical analysis' found in Section 8.7 of this Standard were adopted in this study in order to establish imperfection amplitudes corresponding to quality classes that could realistically be found in practice for a shell structure of this type and slenderness. A total of 19 individual weld depression imperfections were generated, each located at a change of wall strake ('W' in Fig. 1) with the exception of the flanges. Where a weld depression was placed on the boundary of strakes of different wall thicknesses, the average of the two thicknesses was used in the calculation of the imperfection amplitude. The prescribed imperfection amplitudes varied from δ_0/t = 0.36 or δ_0 = 9 mm (Class A), 0.58 or 14.5 mm (Class B) and 0.9 or 22.5 mm (Class C) at the base of the tower, to δ_0/t = 0.55 or δ_0 = 7.7 mm (Class A), 0.88 or 12.32 mm (Class B) and 1.35 or 18.9 mm (Class C) respectively at the top of the tower, the deeper amplitudes being due to a increasing local wall thickness t. A graded mesh was created to ensure a sufficiently fine element resolution near the imperfections to correctly capture local shell bending effects.

4. Modal analysis and sensitivity study

A modal analysis was performed first to extract the vibration modes and associated frequencies of the tower. The fundamental period corresponding to a global cantilever flexure mode was 2.09 s (0.48 Hz), matching very closely with the prediction of a simple average-thickness 'flagpole' with a lumped end mass model. Additionally, a prior field testing programme carried out on a full-scale in-situ tower of this design [47], where ambient vibrations of the structure were measured using long-range Laser Doppler Vibrometers and accelerometers, found the natural frequency to be 0.486 Hz, in very close agreement with the present numerical predictions.

The first (2.09 s) and second (0.24 s) global flexure modes are followed by the first 'local' flexure mode (0.15 s) which includes only local cross-sectional distortions. Both global and local flexure modes arise in pairs at the same vibration period, relating to flexure about the two random perpendicular axes X and Z transverse to the tower. Frequencies associated with local flexure modes, highly dependent on the wall thicknesses, stiffening flanges and mesh, arise in clusters, with higher order modes increasingly concentrated within individual strakes. The first torsional and vertical (Y axis) vibration modes were found to have periods of 0.14 s and 0.09 s respectively, with the first vertical mode in particular controlling the majority of the response of the structure under the vertical component of an earthquake. The influence of weld imperfections on the most important modes was found to be negligible (Fig. 3), the relative difference with respect to the perfect tower being less than 1% for the most imperfect FTQ Class C. The circumferential wave form is not activated in the global flexural modes due to the presence of the stiffening flanges (Fig. 1), which act as restraints for out-of-round displacements.

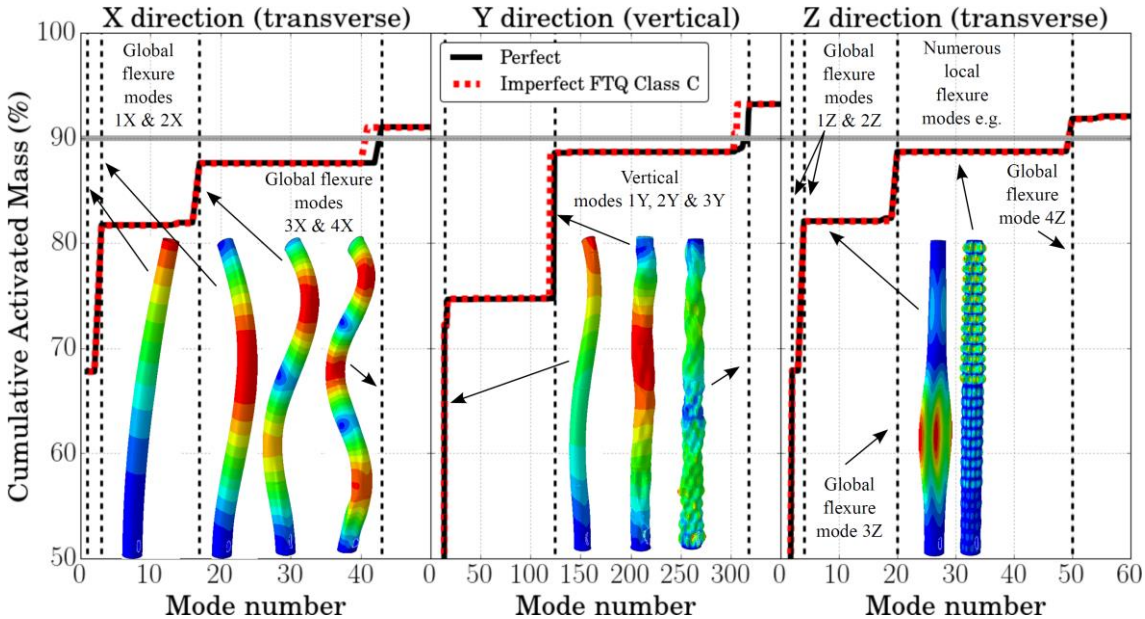

Fig. 3 – Vibration modes and percentage cumulative activated masses in three directions (X & Z transverse, Y vertical) as a function of the vibration mode *N*, shown for perfect and most imperfect structures (FTQ Class C)

An analysis of the accumulated activated masses (Fig. 3) shows that the first two horizontal modes activate more than the 80% of the mass in either transverse direction, with 50 vibration modes being sufficient to activate more than 90%. The first vertical

mode (14^{th}) activates 75% of the mass in the vertical direction, however almost 320 computed modes would need to be included to activate 90% of the mass in the vertical direction and thus strictly meet typical code requirements [27], a figure attributed to the substantial axial membrane stiffness of a near-cylindrical shell. The vast majority of these 320 modes are high-order local flexure modes that add only incrementally to the mass and are very sensitive to the resolution of the finite element mesh. It was therefore decided to relax the code requirements and limit the number of vibration modes to be considered in the analyses to the first 50 computed modes only. These are used to define the Rayleigh damping parameters, affecting the frequencies from 0.48 to 22.6 Hz only, and the maximum analysis step time Δt_{max}.

The MSAs that follow use the implicit Hilber-Hughes-Taylor (HHT) time integration algorithm [23] to directly integrate the system of equations without adopting a modal decomposition approach. HHT permits a variable time step Δt that is automatically reduced to aid convergence in the event of significant material and geometrical nonlinearities. The maximum value of Δt, Δt_{max}, is set according to the accelerogram step time and the highest (50^{th}) vibration mode of interest. An initial sensitivity study found that the displacement and energy responses obtained by adopting the Δt_{max} of the accelerogram record (0.005 or 0.01 s) rather than a smaller $\Delta t_{max} \approx 0.0044$ s (i.e. 10% of the vibration period of the highest mode of interest [48], or 1/22.6 s) were very similar. Consequently, Δt_{max} was taken as equal to the time step of the accelerogram record which, while avoiding information loss, permits accurate modelling of the structural response under the governing vibration frequencies (at least 100, 12 and 5 analysis increments are conducted per cycle of the 1^{st} horizontal, 2^{nd} horizontal and 1^{st} vertical vibration modes respectively) at a tolerable computational cost.

5. Seismic actions and Intensity Measures

The proposed seismic action distinguishes between 'near-fault' (NF) and 'far-field' (FF) records in two essential aspects. Firstly, the selected NF records include distinct velocity pulses not present in the FF records which are known to maximise the potential damage to the structure [49]. Secondly, NF records have strong vertical accelerations in comparison with the two horizontal components. It should be noted that the focus is on the potential impact of these two characteristic features of NF records on the seismic response of slender towers with imperfections, and not on the rupture distance (below 10 km for NF records and between 15 and 50 km for FF records) or the spectrum shape.

Twenty representative triaxial accelerograms, ten NF and ten FF, were extracted from the Pacific Earthquake Engineering Research Centre – National Ground Acceleration database (PEER – NGA-West 2 [50]) for use in the MSAs that follow. The relevant seismological information and first mode spectral accelerations of the unscaled original records (considering $\xi = 1\%$) are summarised in Table 1. The moment magnitude (M_w) was selected to vary between 6.5 and 7.5 and the average Joyner-Boore (R_{jb}) distances are 4.1 and 30 km in the NF and FF records respectively. The unscaled acceleration spectra ($\xi = 5\%$) and positions of respective fundamental periods are illustrated in Fig. 4. The respective spectra will subsequently be scaled in the MSAs using the same scale factor k for all three direction components X, Y and Z.

The average significant duration $D_{5\text{-}95\%}$ of the selected signals is 11.5 and 29.3 s for the NF and FF ground motions respectively, reflecting the faster energy release in NF

earthquakes. The strong motion window was extended in the analyses to include the interval between the 0th and 95th of the cumulative Husid Plot, i.e. $D_{0\text{-}95\%}$. In comparison with the total duration of the record ($D_{0\text{-}100\%}$), using $D_{0\text{-}95\%}$ substantially reduces computational cost of each one of the vast set of nonlinear dynamic analyses that needed to be performed, whilst still taking the full wave-train record into account [51]. Though the soil class was not a criterion, the average shear-wave velocity over the upper 30 m ($V_{s,30}$) of the selected records is consistent with dense sand, gravel or stiff clay [26]. The exception is Pacoima Dam which is consistent with a rock formation.

As the dynamic response of wind turbines is dominated by fundamental modes (Fig. 3), the spectral acceleration at these periods along a specific direction of the structure (e.g. $S_a^j(T_1^j)$ where j = X, Y or Z) in principle offers an efficient Intensity Measure (IM) [52]. This IM is direction and ξ-specific and may be taken as the geometric average of the spectral accelerations in the random transverse directions X and Z, with or without the vertical direction Y as required:

$$S_a^{XZ}\left(T_1\right)=\left[S_a^X\left(T_1^X\right)\times S_a^Z\left(T_1^Z\right)\right]^{1/2} \tag{2a}$$

$$S_a^{XYZ}\left(T_1\right)=\left[S_a^X\left(T_1^X\right)\times S_a^Y\left(T_1^Y\right)\times S_a^Z\left(T_1^Z\right)\right]^{1/3} \tag{2b}$$

The proposed IMs are not affected by the weld imperfections as these have been found to have only a negligible influence on low-order vibration modes (Fig. 3). Note the following in Eq. 2: $T_1^X = T_1 \approx 2.09$ s, $T_1^Z = T_2 \approx 2.09$ s and $T_1^Y = T_{14} \approx 0.09$ s.

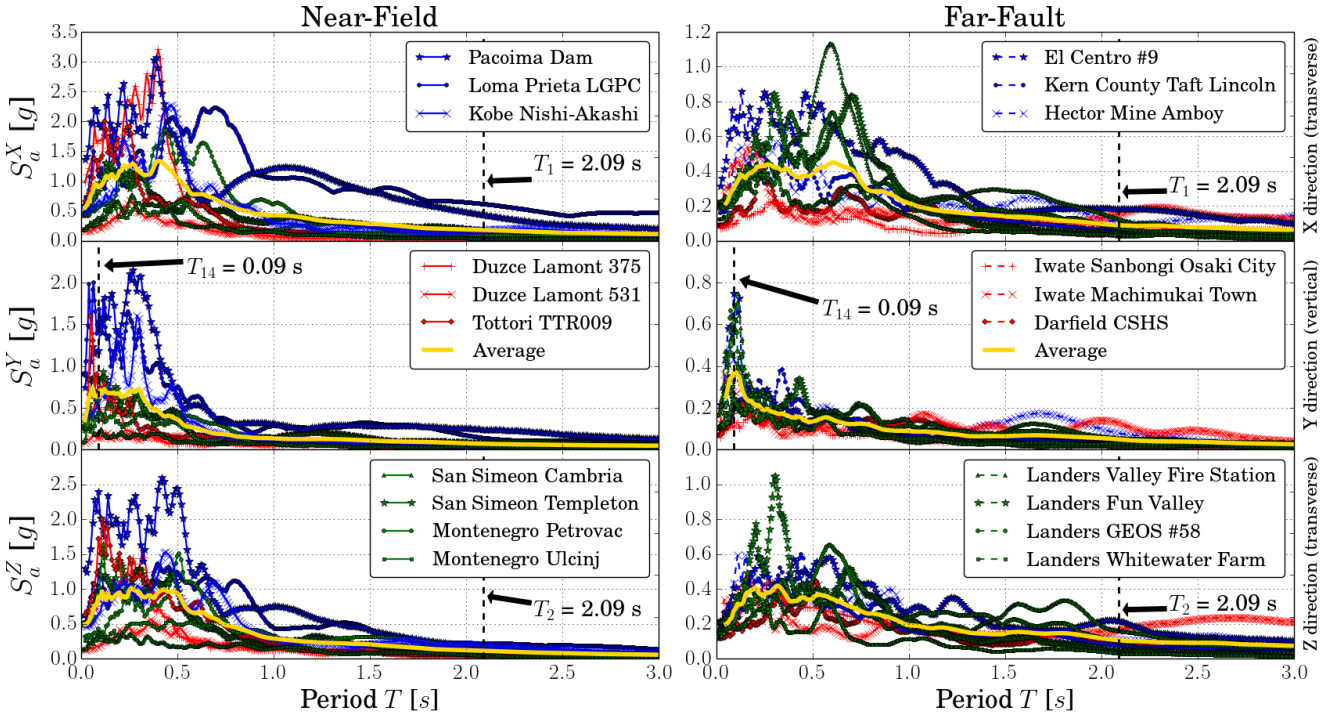

Fig. 4 – Triaxial acceleration spectra of unscaled records considered in this study assuming a damping ratio of ξ = 5%. The fundamental vibration periods of the structure in the three directions are marked with dashed lines.

Table 1 – Seismological information and 1% damping spectral accelerations at fundamental periods for the natural records employed in MSAs

	Record / station, year	M_w	V_{s30} [m/s]	$D_{5\text{-}95\%}$ [s]	$S_a^j(T_1^j)$ [g]			$S_a^{XZ}(T_1)$ [g]	$S_a^{XYZ}(T_1)$ [g]
					j = X	j = Y	j = Z		
NF	San Fernando / Pacoima Dam, 1971	6.6	2016.1	7.3	0.47	2.13	0.17	0.28	0.55
	Loma Prieta / LGPC, 1989	6.9	594.8	10.2	0.70	1.75	0.25	0.42	0.67
	Kobe / Nishi-Akashi, 1995	6.9	609.0	11.2	0.27	0.81	0.23	0.25	0.37
	Duzce / Lamont 375, 1999	7.1	454.2	13.1	0.04	0.92	0.04	0.04	0.11
	Duzce / Lamont 531, 1999	7.1	683.4	14.9	0.03	0.21	0.03	0.03	0.05
	Tottori / TTR009, 2000	6.6	420.2	11.1	0.19	0.95	0.06	0.11	0.22
	San Simeon / Cambria, 2003	6.5	362.4	13.2	0.04	0.49	0.06	0.05	0.11
	San Simeon / Templeton, 2003	6.5	410.7	10.3	0.21	1.24	0.22	0.22	0.39
	Montenegro / Petrovac, 1979	7.1	543.3	13.3	0.13	0.62	0.09	0.11	0.19
	Montenegro / Ulcinj, 1979	7.1	410.3	12.2	0.13	0.73	0.24	0.18	0.28
	Geometric average	6.8	562.3	11.5	0.13	0.85	0.11	0.15	0.23
FF	Imperial Valley / El Centro, 1940	6.9	213.4	24.2	0.23	1.11	0.37	0.29	0.46
	Kern County / Taft Lincoln, 1952	7.4	385.4	30.3	0.09	0.38	0.11	0.10	0.15
	Hector Mine / Amboy, 1999	7.1	382.9	26.7	0.24	0.81	0.14	0.18	0.30
	Landers/Valley Fire Station, 1992	7.3	396.4	31.9	0.22	1.04	0.19	0.21	0.35
	Landers / Fun Valley, 1992	7.3	388.6	29.6	0.07	0.34	0.07	0.07	0.12
	Landers / GEOS #58, 1992	7.3	368.2	32.9	0.13	1.00	0.18	0.15	0.29
	Landers / Whitewater Farm, 1992	7.3	425.0	33.4	0.07	0.62	0.05	0.06	0.13
	Iwate / Sanbongi Osaki City, 2008	6.9	539.9	29.1	0.14	0.21	0.18	0.16	0.17
	Iwate / Machimukai Town, 2008	6.9	655.4	27.3	0.19	0.41	0.20	0.19	0.25
	Darfield / CSHS, 2010	7.0	638.4	28.9	0.06	0.44	0.15	0.10	0.15
	Geometric average	7.1	420.2	29.3	0.13	0.55	0.14	0.14	0.22

The vertical spectral acceleration associated with the first vertical vibration mode $S_a^Y(T_1^Y)$ is significantly larger than that in the horizontal directions $S_a^X(T_1^X)$ or $S_a^Z(T_1^Z)$. The smaller period of the first vertical mode (0.09 s) places the structure in the region of the spectrum with large vertical accelerations, whereas the large period of the first global flexure mode (2.09 s) is associated with smaller accelerations. It is clear from Table 1 that the ratio between the vertical acceleration associated with the first vertical mode for the NF records and the averaged IM in the horizontal direction (considering in both cases the geometric average of the set of 10 records of the same type of earthquake) is much higher for the NF records where $S_a^Y(T_1^Y)$ / $S_a^{XZ}(T_1)$ = 5.7 compared with the FF records for which this ratio is 3.9. Despite the reduced participation factor of the vertical modes, their high spectral accelerations may contribute the seismic response of slender and imperfection-sensitive shell structures such as wind turbine support towers, as is investigated further in the next section.

6. Time-history and multiple stripe analyses

The multiple stripe analysis (MSA) is characterised by Intensity Measures (IM) and Engineering Demand Variables (EDV) that represent the structural response for different levels of the seismic intensity [53,54]. This section begins by illustrating EDVs appropriate for the three-dimensional seismic analysis of wind turbine support towers and presents the results of the MSAs under the varying influence of the vertical earthquake component, geometric imperfections, NF vs FF records and damping.

6.1. Engineering Demand Variables (EDVs)

One EDV considered in this study is the peak of the lateral drift, calculated as the square root of the sum of the squares of the displacements in the transverse X and Z directions at the top of the tower ('T' in Fig. 1) in the interval $D_{0\text{-}95\%}$ and divided by the height of the support tower (~61.8 m). A second energy-based EDV is used to complement the information obtained from drifts and to explore the hysteretic behaviour of the structure in the inelastic range: it is taken as the accumulated plastic energy dissipated by the structure (E_{sp}) at the end of each analysis at $t = D_{0\text{-}95\%}$ [55,56].

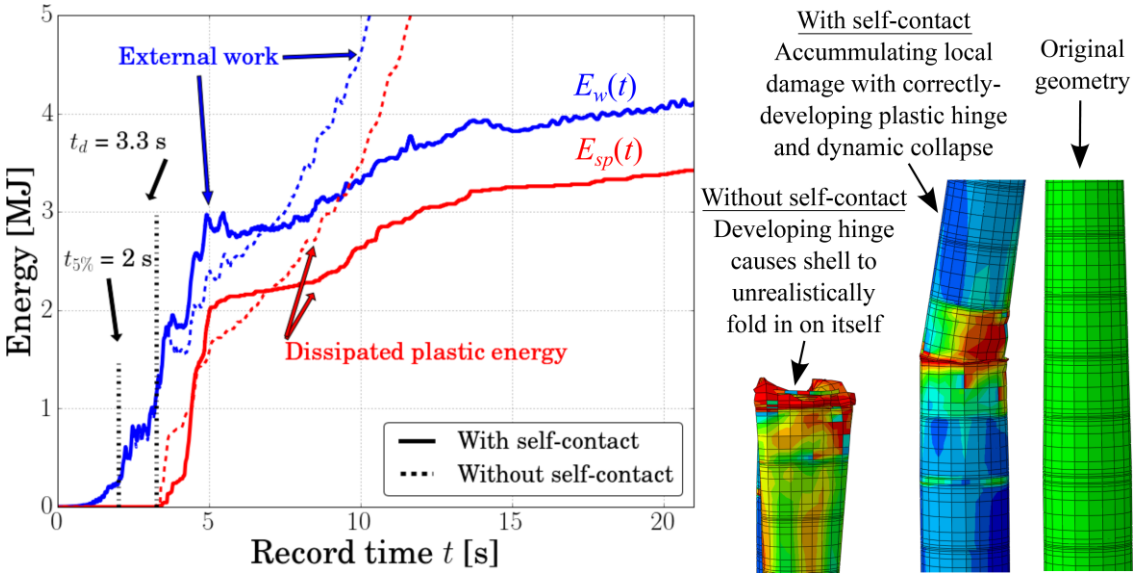

Fig. 5 – External work and energy dissipated by plasticity for models with and without self-contact (El Centro #9, perfect shell, ξ = 1%, $S_a^{XYZ}(T_1) \approx 2$ g)

The reason for including self-contact in the FE model can now be explained. At high ground accelerations, the wind turbine support tower suffers dynamic collapse through the development of a plastic hinge at a variable location, though always at a change of wall strake or weld depression. When the finite elements do not detect self-contact, the material overlaps and the shell effectively folds in on itself during collapse, leading to a wholly unrealistic response (Fig. 5). With self-contact included, illegal deformations are arrested as the shell detects other portions of itself during collapse, leading to a more realistic plastic hinge development and a monotonic increase in absorbed plastic energy, and thus a more realistic energy balance at the end of the modelled record. It should be stressed that such nonlinear contact analyses are highly discontinuous and computationally intensive, a property that would only be exacerbated by including a more complex contact model, say with a finite 'dry' friction rule, for which reliable material data is difficult to determine and therefore lies outside the scope of this study.

The lower bound for the dissipated plastic energy is zero, indicating a completely elastic response. However, the response is always elastic at the start of the structural motion and the onset of the plastic dissipation is delayed. The interval of strong pulses starts approximately at $t_{5\%}$ (5th percentile of the cumulative Husid plot), as illustrated in Fig. 5 on the El Centro #9 record scaled to $S_a^{XYZ}(T_1) \approx 2$g. Though the external work introduced by the earthquake begins to rise greatly at $t_{5\%} \approx 2$ s, plastic dissipation does not start here until $t_d \approx 3.3$ s at which point the curve corresponding to the external work E_w rises in tandem with the plastic dissipated energy E_{sp} to eventually attain a plateau. This signifies that once a hinge develops in the tower, any further input in

seismic energy is largely dissipated by plasticity at the hinge. The magnitude of the time delay in the plastic dissipation $\Delta t_d = t_d - t_{5\%}$ controls the portion of the total external work dissipated by plasticity, which accordingly depends on the ground motion, the structural response and damping ratio ξ.

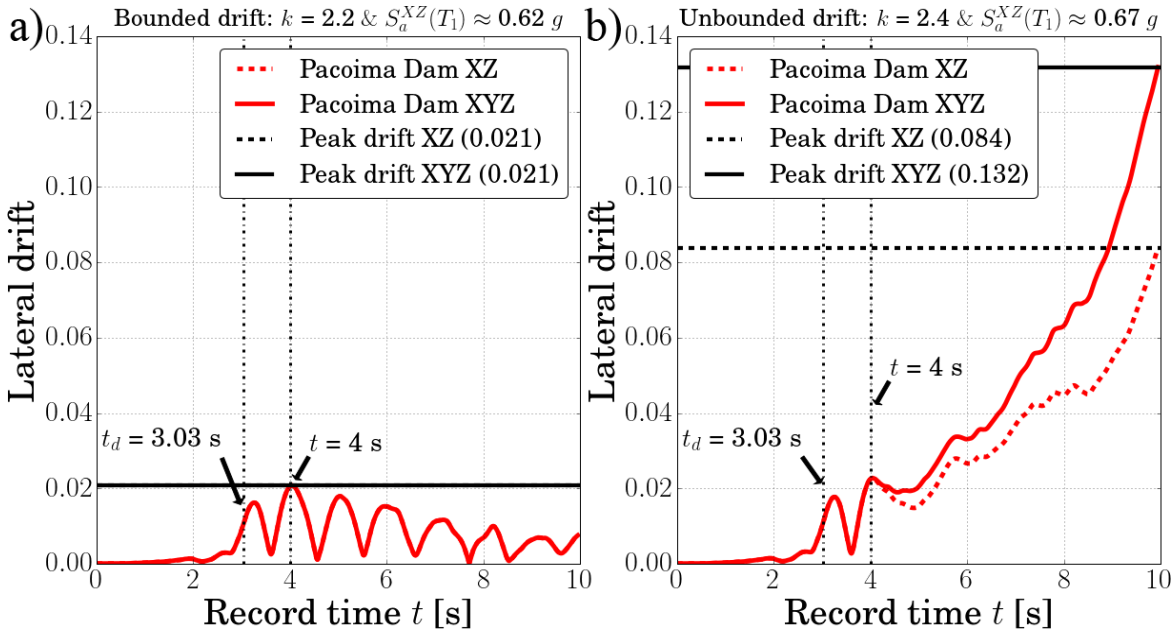

Fig. 6 – Time-history response of the lateral drift with (XYZ) and without (XZ) the vertical acceleration component (Pacoima Dam, perfect shell, ξ = 1%, $S_a^{XZ}(T_1) \approx 0.62$ g and 0.67 g respectively)

The peak lateral drift is independent of the earthquake duration [57]. For the Pacoima Dam record scaled by a factor of k = 2.2 (Fig. 6a), for example, the structure remains globally stable throughout and a finite peak drift is observed at $t \approx 4$ s, within the reduced record duration $D_{0\text{-}95\%}$ and close to the time of the peak ground acceleration. By contrast, an only slightly higher scale factor of k = 2.4 causes global dynamic collapse through the formation of a plastic hinge (Fig. 6b) and an apparent unbounded growth in drift. In this case, the peak lateral drift is undefined and a value 'off the scale' will be shown in the MSA curves which follow to represent a state of collapse.

6.2. Influence of the vertical earthquake motions and varying imperfection amplitudes

A growing body of research suggests that vertical motions may be detrimental to the seismic response of certain structures [58]. As cylindrical shells are known to be sensitive to axial loading, this hypothesis is investigated here by analysing the behaviour of an increasingly imperfect tower (decreasing FTQ Class) under three representative records, Pacoima Dam, Duzce Lamont 375 and El Centro #9, both with and without their vertical acceleration components. The computed MSA curves for ξ = 1% are first presented in terms of the IM against the peak lateral drift (Fig. 7), with horizontal lines representing a state of dynamic collapse, and again in terms of the total accumulated plastic energy dissipated at $t = D_{0,95\%}$ (Fig. 8). As vertical accelerations were not included in each analysis for this part of the study, the IM was taken as $S_a^{XZ}(T_1)$ (Eq. 2a).

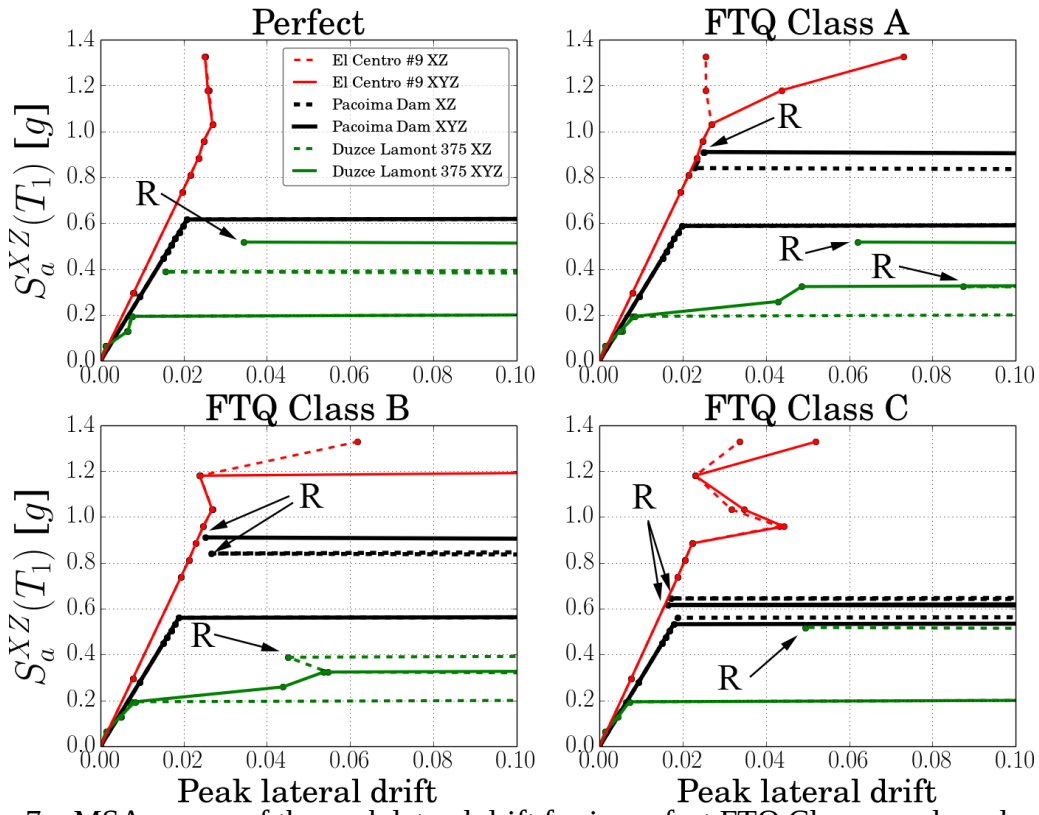

Fig. 7 – MSA curves of the peak lateral drift for imperfect FTQ Classes under selected records without (XZ) and with (XYZ) the vertical acceleration component (ξ = 1%); 'R' denotes an instance of structural resurrection

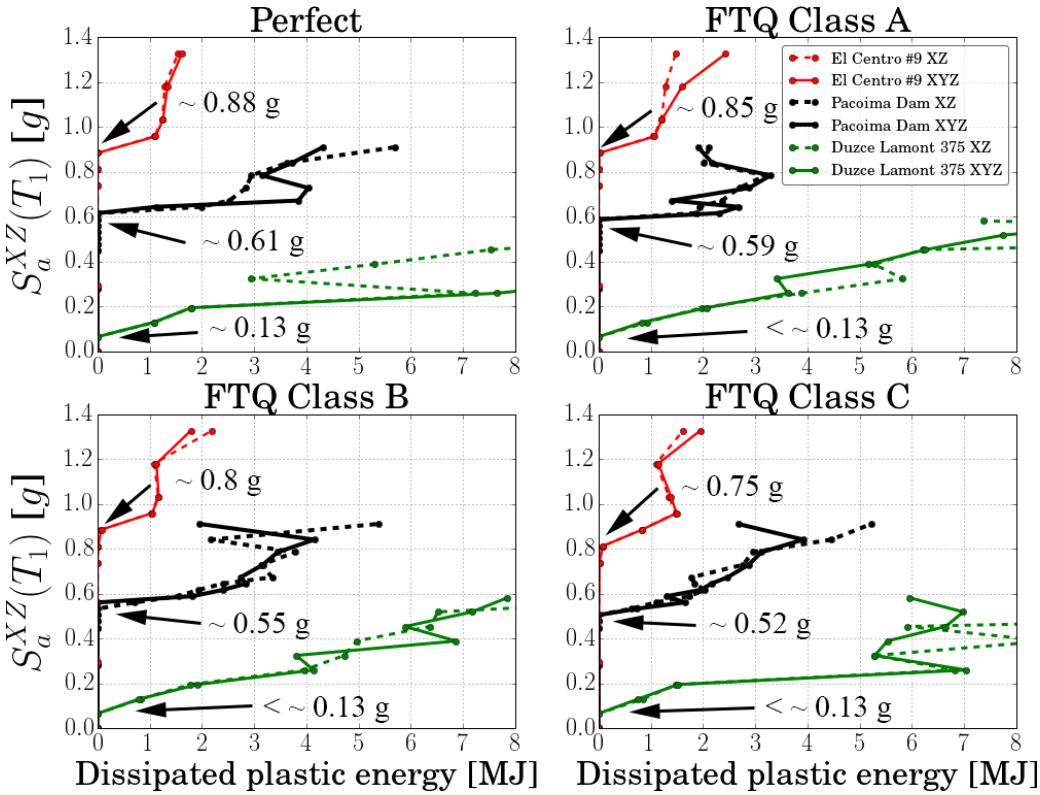

Fig. 8 – MSA curves of the dissipated plastic energy at $t = D_{0\text{-}95\%}$ for different imperfect FTQ Classes under selected records without (XZ, dashed lines) and with (XYZ, solid lines) the vertical acceleration component (ξ = 1%)

When the response is elastic, the influence of the vertical component appears negligible even for the most imperfect structure with no plasticity energy dissipation. Once plasticity initiates, only a small increase in the IM is sufficient to cause the dissipation energy to rise greatly. This damaged state corresponds to the presence of a plastic hinge at a change of wall thickness or weld imperfection or both, at which point the structure is undergoing dynamic collapse. This echoes the findings of Nuta *et al*. [3] who advise high safety factors against any overloading because of the risk of sudden collapse when the tower is excited beyond its elastic limit. Further, neither the vertical component nor the imperfection amplitude appears to have a significant influence on the dissipated plastic energy at $t = D_{0\text{-}95\%}$ for any record. The Duzce Lamont 375 record deserves particular mention, as it appears to be especially damaging to the structure causing plastic damage even at very low IMs. Its velocity spectrum (Fig. 9) exhibits a distinct peak close to the vibration periods of the second pair of global flexure modes (0.24 s) and, as a result, a very early formation of a plastic hinge at $S_a^{XZ}(T_1)$ of ~0.13 g is observed. It is also noted that the potential elongation of the second-order periods due to structural damage may also contribute to strong increments in the seismic input.

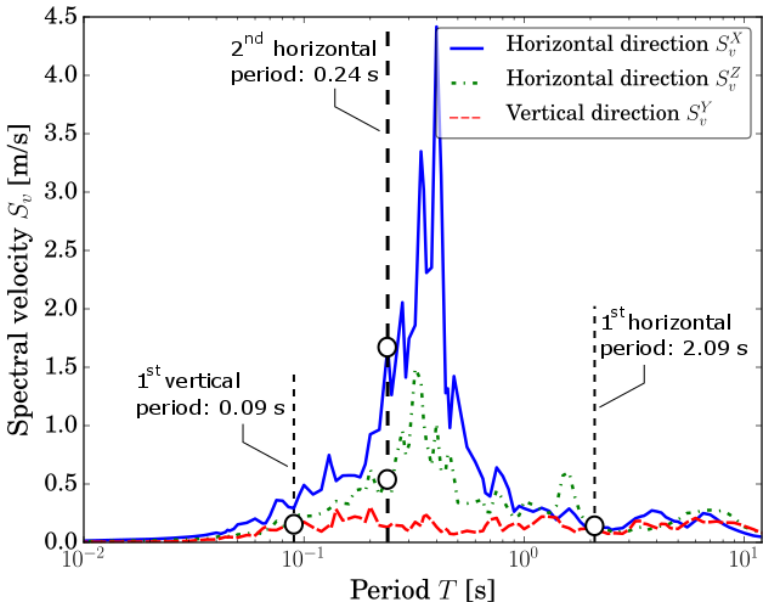

Fig. 9 – Triaxial velocity spectra of unscaled Duzce Lamont 375 record (ξ = 1%), with relevant vibration periods of the structure are marked with dashed lines

The most important effect of the weld depression imperfections, with or without the additional vertical ground acceleration, is to significantly lower the level of the IM that initiates the nonlinear response. As is highlighted in Fig. 8, this occurs at ~0.61 g for the perfect structure under the Pacoima Dam record, dropping to ~0.59 g, ~0.55 g and ~0.52 g for FTQ Classes A, B and C respectively, while for the El Centro #9 record these IMs are ~0.88 g, ~0.85 g, ~0.8 g and ~0.75 g respectively. This means that in moving from the traditional analysis of a perfect wind turbine tower to the most imperfect considered structure, the IM of the earthquakes at which damage initiates is reduced by 17%. It is therefore important to include realistic geometric imperfections in structures known to be sensitive to them, particularly where the boundary between the onset of damage and total collapse is so slim.

A further effect is that these imperfections appear to increase the variability in the seismic response, particularly regarding the location of the plastic hinge. The hinge locations are illustrated schematically for the Duzce Lamont 375 record in Table 2, both with and without the vertical component, for which it was observed that they form exclusively within the upper portion of the tower (Fig. 1). The perfect structure has only one geometric discontinuity in this region, namely the abrupt drop in local wall stiffness caused by a stepwise change in thickness from 10 to 11 mm (location A in the embedded diagram within Table 2), and thus only one potential hinge location. By contrast, the imperfect tower has nine weld depressions and thus nine potential hinge locations in this region, though under the Duzce Lamont 375 record only two appear to be critical (interchangeably locations B and C but, interestingly, not A). The plastic hinge location appears liable to change when the vertical acceleration component is included, but since in this particular design the upper regions are uniformly 10 mm thick and therefore approximately equally strong, the response under the records shown here does not appear to be significantly affected. The relative insensitivity of the response to the vertical acceleration component further suggests that it is above all the additional compression induced by global bending under horizontal inertia forces that is critical for stability. It is important to stress that other tower designs may have very different wall thickness and d/t distributions, and the possibility of vertical accelerations precipitating a plastic hinge at a weaker junction should not be discounted. Indeed, though not shown here due to space constraints, in the study of the full set of NF and FF records the tower was found to develop hinges at most wall discontinuities (13 and 22 for perfect and imperfect structures respectively).

Lastly, it is interesting to note the possibility that ever more intensive ground accelerations are not necessarily more deleterious to the structure beyond the elastic limit. A small increase in the IM may significantly reduce the peak recorded drift and, though it does not necessarily eliminate the plastic hinge, causes it to form sooner in time which helps 'protect' the structure from subsequent acceleration peaks. This hardening behaviour (or 'structural resurrection'; marked with an 'R' in Fig. 7) has previously been observed in multi-storey steel moment-resisting frames [53]. However, it should be stressed that cantilever shell structures appear particularly prone to large surges in the peak drift for only small increases in IM due to their structural simplicity, this sudden softening behaviour corresponding to dynamic collapse.

Table 2 – Plastic hinge locations for the Duzce Lamont 375 record without (XZ) and with (XYZ) the vertical acceleration component (ξ = 1%) (see also Fig. 1)

$S_a^{XZ}(T_1)$ [g]	Perfect		FTQ Class A		FTQ Class B		FTQ Class C		
	XZ	XYZ	XZ	XYZ	XZ	XYZ	XZ	XYZ	
0.07	n/a	n/a	n/a	n/a	n/a	n/a	n/a	n/a	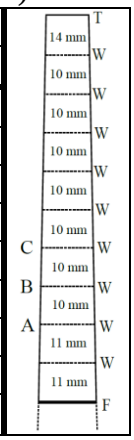
0.13	A	A	C	C	C	C	B	C	
0.20	A	A	B	B	B	B	B	B	
0.26	A	A	B	B	B	C	B	B	
0.33	A	A	B	B	B	B	B	B	
0.40	A	A	B	B	B	B	B	B	
0.46	A	A	B	B	B	B	B	B	
0.53	A	A	B	B	C	B	B	B	
0.59	A	A	C	B	C	B	B	B	

6.3. Aggregate response under representative near-fault and far-fields records

The different response under 'near-fault' (NF) and 'far-field' (FF) records, and the influence of damping (ξ = 1% and 5%)) on the damage are illustrated here on the perfect and most imperfect structures (FTQ Class C). As the vertical acceleration component was included in all analyses presented here, the IM was taken as $S_a^{XYZ}(T_1)$ (Eq. 2b). The computed MSA curves are presented in terms of this IM against the peak lateral drift (Fig. 10) and the accumulated dissipated plastic energy at $t = D_{0\text{-}95\%}$ (Fig. 11). Both are represented by the mean value at each intensity level assuming a lognormal distribution, with NF and FF records aggregated separately. The asymmetric dispersions about the mean are represented by 95% Confidence Intervals (CIs). Note that only bounded drifts have been considered in the mean and CIs for any IM, with unbounded drifts signifying dynamic collapse removed from the calculation (Fig. 6).

The aggregate levels of dissipated plastic energy suggest that damage in the perfect structure begins on average at an IM of ~1.3 g for the NF records and ~1.6 g for the FF records assuming ξ = 1%, while for the imperfect structure this drops significantly to ~1.15 g and ~1.25 g respectively, closely reflecting the findings presented in Fig. 8. Further, when scaled to the same IM, the NF records are significantly more demanding than FF records, as manifest by higher mean drifts and dissipated plastic energies. This may be explained by the presence of distinct velocity pulses in NF records, but not FF records, affecting the dominant global flexure modes of the structure. The Duzce Lamont 375 record (and to a lesser extent Lamont 531) was again found to exhibit by far the most damaging response among the NF set due to the presence of a high-energy velocity pulse exciting the second pair of global flexure modes (Fig. 9).

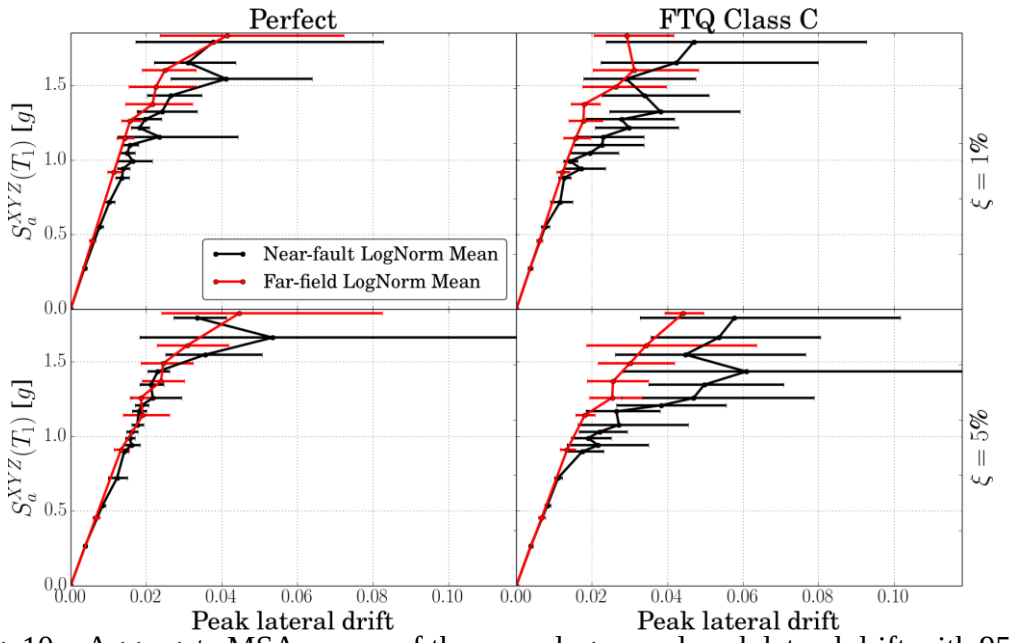

Fig. 10 – Aggregate MSA curves of the mean lognormal peak lateral drift with 95% Confidence Intervals for the perfect and most imperfect structure

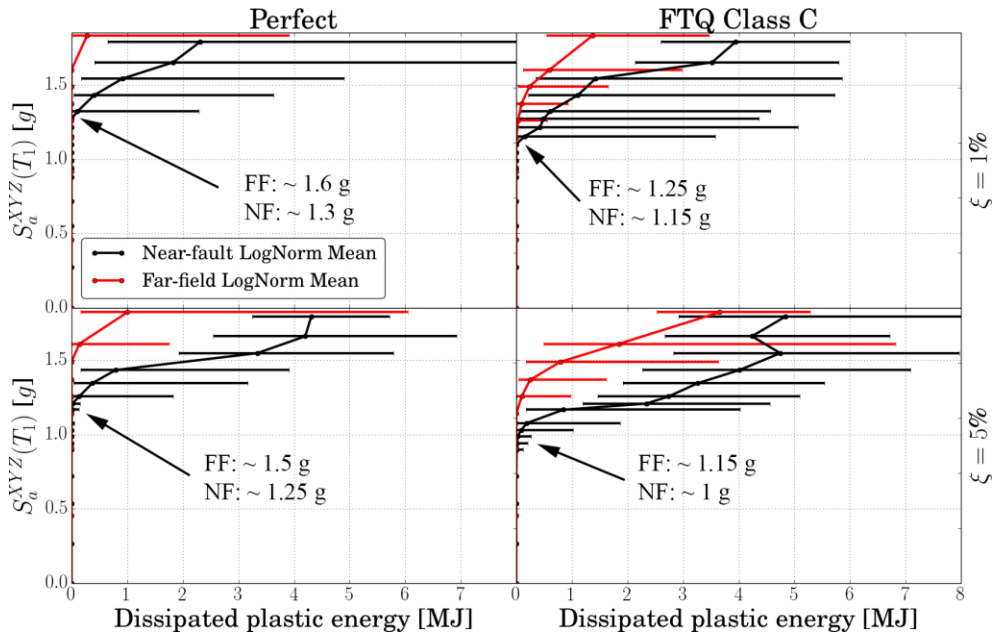

Fig. 11 – Aggregate MSA curves of the mean accumulated dissipated plastic energy at $t = D_{0\text{-}95\%}$ with 95% Confidence Intervals for the perfect and most imperfect structure

It is interesting to note that for the same seismic intensity the structure appears to suffer significantly higher levels of drift and plastic damage for ξ = 5% than 1%. This is attributed to different scaling factors k employed to achieve the same IM for 1% and 5%-damped spectra, and to the smoothing effects of larger damping values on the corresponding spectral shape. Although the IM definition employed here aims to attain consistent earthquake acceleration levels along different directions (Eq. 2b), it does not guarantee an exact equivalence of spectral ordinates at individual periods or at other spectral quantities such as displacements. This is illustrated in Fig. 12a on the Montenegro Ulcinj record where scale factors of 5.45 and 7.7 have been applied to the ξ = 1% and 5% records to scale them to $S_a^{XYZ}(T_1) \approx 1.54$ g respectively, causing the spectral displacements S_d at the fundamental period T_1 = 2.09 s to be consistently higher for ξ = 5% than 1%. This causes larger drifts in the elastic range at ξ = 5% and an early onset of a plastic hinge with higher levels of dissipated plastic energy over the course of the record (Fig. 12b).

It is of course possible, given the jagged nature of spectral representation, that for other record combinations the opposite elastic behaviour takes place (i.e. larger initial displacements leading to earlier hinge formation for ξ = 1% than 5%). However, the tendency of very stiff structures with negligible damping and significant strength degradation to undergo oscillations around zero drifts, as opposed to the marked unsymmetrical ratcheting response observed for the same structures for relatively mild values of additional energy dissipation [59], may contribute towards 5%-damped structures experiencing consistently larger drifts and plastic damage levels. These phenomena are further manifest in the lower IMs at which mean plasticity rises above zero at ξ = 5% than at 1% for both NF and FF records, and in wider 95% CIs for the imperfect structure (Figs 9 and 10). The latter is due to weld depression imperfections increasing the variability in the potential hinge locations (e.g. Table 2), more likely to form due to higher drifts at ξ = 5% than 1%. The sensitivity of the seismic response to the structural damping and the uncertainties associated with its estimation and modelling should be investigated in further studies.

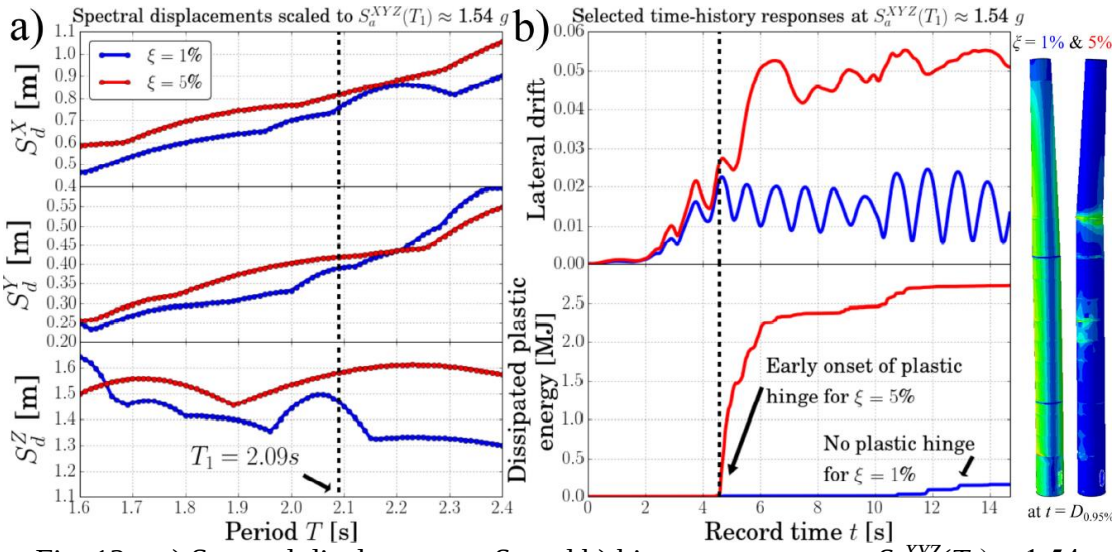

Fig. 12 – a) Spectral displacements S_d and b) history responses at $S_a^{XYZ}(T_1) \approx 1.54$ g, scaled by $k = 5.45$ and 7.5 for $\xi = 1$ and 5% respectively (Montenegro Ulcinj, perfect)

7. Conclusions

This paper presents an extensive set of nonlinear history response analyses investigating the seismic behaviour of a slender metal wind turbine support tower, modelled as a thin-walled near-cylindrical shell, under a representative selection of ten 'near-fault' and ten 'far-field' earthquake records. The following findings are offered:

- The tower exhibits high membrane stiffness against seismic excitations, but once in the inelastic range a plastic hinge develops at a change of thickness potentially leading to catastrophic collapse, with very little prior energy dissipation and no alternate load paths.

- The imperfections of the wall significantly reduce (up to 17%) the spectral acceleration at which plastic damage initiates. An imperfect tower also exhibits more numerous potential hinge locations, increasing the variability in the seismic response.

- The inclusion of vertical accelerations is not necessarily more detrimental to the elastic response or the intensity at which damage initiates. However, it has the potential to shift the critical hinge location to a weaker part of the tower, particularly when imperfections are present.

- When scaled to the same spectral acceleration at fundamental periods, near-fault records with pulse-like effects and large vertical accelerations are more demanding in wind turbine towers with imperfections than far-fault records with rupture distances below 50 km.

- A preliminary investigation into the effects of scaling to attain target average spectral accelerations from spectra with different damping levels suggests that employing higher damping may be more damaging to the structure. This is attributed to differences in spectral ordinates at individual periods leading to larger scaled spectral displacements at the fundamental period and the proneness of the structure to ratcheting collapse.

- Wind-turbines are dominated by the fundamental modes and the Intensity Measure based on the geometric average of the spectral acceleration at the first periods in the three directions is a reasonable choice for multiple stripe analyses. However, further studies are necessary to investigate the efficiency of Intensity Measures that incorporate selected higher order modes.

8. Recommendations

The present exploratory study permits only limited specific design advise at this stage, but the following recommendations may be made relating to the analysis and design of wind turbine towers under seismic excitations:

- Given the lack of structural redundancy of these structures and the shared weakness in wind farms, high factors of safety are recommended against seismic loads, even if these are often considered of secondary importance compared to wind loading.

- Realistic weld depression imperfections at every change of wall thickness should be included in the realistic seismic risk assessment of wind-turbines, due to the susceptibility to total collapse after the formation of just one plastic hinge. Special attention should be paid during construction to ensure tight tolerances are met (i.e. the tower adheres to the best possible FTQ Class), as deeper imperfections increase the risk of sudden collapse.

- Capturing the nonlinear response of such a slender metal shell structure accurately requires modelling of the local wall self-contact that arises due to the development of a plastic hinge. A simple 'frictionless' tangential and 'hard' normal contact model was assumed here for computational efficiency, though further studies should be made to explore these assumptions.

- A detailed analysis of the response of the tower under near-fault records with possible velocity pulses containing vibration with periods close to the first and second global flexure vibration modes is recommended if the wind farm ia located in the proximity of an active fault.

- Regardless the rupture distance of the records and the presence or not of pule-like effects, their vertical component should be included in seismic assessments of such structures.

References

[1] GWEC (2014a) "Global wind report – Annual market update 2014" *Corporate Publication by the Global Wind Energy Council*.

[2] GWEC (2014b) "Global wind energy outlook 2014" *Corporate Publication by the Global Wind Energy Council (GWEC) and Greenpeace*.

[3] Nuta E., Christopoulos C. & Packer J.A. (2011) "Methodology for seismic risk assessment for tubular steel wind turbine towers: application to Canadian seismic environment" *Canadian Journal of Civil Engineering*, 38, 293-304.

[4] Myers A.T., Gupta A., Ramirez C.M. & Chioccarelli E. (2012) "Evaluation of the seismic vulnerability of tubular wind turbine towers" *Proc. 15th World Conf. Eqk. Eng.*, 24-28 Sep., Portugal.

[5] Thomsen K. & Sørensen P. (1999) "Fatigue loads for wind turbines operating in wakes" *Jrnl. of Wind Eng. & Ind. Aerodynamics*, 80, 121-136.
[6] Riziotis V.A. & Voutsinas S.G. (2000) "Fatigue loads on wind turbines of different control strategies operating in complex terrain" *Jrnl. of Wind Eng. & Ind. Aerodynamics*, 85, 211-240.
[7] Maalawi K.Y. & Negm H.M. (2002) "Optimal frequency design of wind turbine blades" *Jrnl. of Wind Eng. & Ind. Aerodynamics*, 90(8), 961-986.
[8] Uys P.E., Farkas J., Jármai J. & van Tonder F. (2007) "Optimisation of a steel tower for a wind turbine structure" *Eng. Strct.*, 29, 1337-1342.
[9] Hu Y., Bianotopoulos C. & Yang J. (2014) "Effect of internal stiffening rings and wall thickness on the structural response of steel wind turbine towers" *Eng. Strct.*, 81, 148-161.
[10] Bazeos N.,Hatzigeorgiou G.D.,Hondros I.D.,Karamaneas H.,Karabalis D.L.&Beskos D.E. (2003) "Static, seismic & stability analyses of a prototype wind turbine steel tower" *Eng. Strct.*, 24, 1015-25.
[11] Lavassas I., Nikolaidis G., Zervas P., Efthimiou E., Doudoumis I.N. & Baniotopoulos C.C. (2003) "Analysis and design of the prototype of a steel 1-MW wind turbine tower" *Eng. Strct.*, 25, 1097-1106.
[12] Witcher D.(2005)"Seismic analysis of wind turbines in the time domain"*Wd Enrg*,8,81-91.
[13] Stamatopoulos G.N. (2013) "Response of a wind turbine subjected to near-fault excitation and comparison with the Greek Aseismic Code provisions" *Soil Dyn. & Eqk Eng*, 46, 77-84.
[14] Katsanos E.I., Thons S. & Georgakis C.T. (2016). Wind turbines and seismic hazard: a state-of-the-art review. *Wind Energy*. DOI: 10.1002/we.1968.
[15] EN 1993-1-1 (2005) "Eurocode 3: Design of steel structures, Part 1.1: General rules and rules for buildings" *Comité Européen de Normalisation*, Brussels.
[16] AISC 360-10 (2010) "Specification for Structural Steel Buildings" *Am. Inst. of Steel Con.*
[17] Koiter W.T. (1945) "On the stability of elastic equilibrium" *PhD Thesis*, Delft, Holland.
[18] Koiter W.T. (1963) "The effect of axisymmetric imperfections on the buckling of cylindrical shells under axial compression" *Proc. Kon. Ned. Akad. Wet.*, B66, 265-279.
[19] Yamaki N. (1984) "Elastic stability of circular cylindrical shells" *North-Holland*.
[20] Guo L., Uang C.-M., Elgamal A., Prowell I. & Zhang S. (2011) "Pushover analysis of a 53 m high wind turbine tower" *Advanced Science Letters*, 4, 1-7.
[21] IEC 61400-1 (2005) "Wind turbines – Part 1: Design requirements. 3rd Ed." *International Electrotechnical Commission*, Geneva, Switzerland.
[22] DIN 18800-1 (1990)"Stahlbauten; Bemessung und Konstruktion" *Deutsche Inst für Norm*.
[23] ABAQUS (2014) "ABAQUS Version 6.14-2 Commercial Finite Element Software" *Dassault Systèmes*, Simulia Corporation, Providence, RI, USA.
[24] Gazetas G. (2006) "Seismic design of foundations and soil-structure interaction" *Proc. 1st Europ. Conf. on Earthquake Eng. and Seismology*, 3-8 September, Geneva, Switzerland.
[25] Clough R.W. & Penziem J. (1993) "Dynamics of Structures. 2nd Ed." *McGraw-Hill*.
[26] EN 1998-1 (2004) "Eurocode 8: Design of structures for earthquake resistance, Part 1: General rules, seismic actions and rules for buildings" *CEN*, Brussels.
[27] EN 1998-6 (2005) "Eurocode 8: Design of structures for earthquake resistance, Part 6: Towers, masts and chimneys" *CEN*, Brussels.
[28] Prowell I., Veletzos M., Elgamal A. & Restrepo J. (2009) "Experimental and numerical seismic response of a 65 kW wind turbine" *Journal of Earthquake Eng.*, 13, 1172-1190.
[29] Prowell I., Elgamal A., Romanowitz H., Duggan J.E. & Jonkman J. (2010) "Earthquake response modelling for a parked and operating megawatt-scale wind turbine" *Technical Report NREL/TP-5000-48242*, National Renewable Energy Laboratory, Colorado, USA.
[30] Valamanesh V. & Myers A.T. (2014). "Aerodynamic damping and seismic response of horizontal axis wind turbine towers". *ASCE J. Struct. Eng.*, 140(11), 04014090.
[31] Rotter J.M. & Teng J.G. (1989) "Elastic stability of cylindrical shells with weld depressions" *ASCE Journal of Engineering Mechanics*, 115(5), 1244-1263.
[32] Sadowski A.J. & Rotter J.M. (2014) "Modelling and behaviour of cylindrical shells structures with helical features" *Computers and Structures*, 133, 90-102.
[33] Donnell L.H. (1933) "Stability of thin-walled tubes under torsion" *NACA Report N. 479*.
[34] Pircher M., Berry P.A., Ding X. & Bridge R.Q. (2001) "The shape of circumferential weld-induced imperfections in thin-walled steel silos and tanks." *Thin-Wld. Str*, 39, 999-1014.

[35] Teng J.G., Lin X., Rotter J.M. & Ding X.L. (2005) "Analysis of geometric imperfections in full-scale welded steel silos" *Engineering Structures*, 27, 938-950.
[36] Sadowski A.J., van Es S.H.J., Reinke T., Rotter J.M., Gresnigt A.M., Ummenhofer T. (2015) "Harmonic analysis of initial geometric imperfections in spiral welded steel tubes" *Eng.Str*, 85, 234-248.
[37] Rotter J.M. & Zhang Q. (1990) "Elastic buckling of imperfect cylinders containing granular solids" *ASCE Journal of Structural Engineering*, 116(8), 2253-2271.
[38] Knödel P., Ummenhofer T. & Schulz U. (1995) "On the modelling of different types of imperfections in silo shells" *Thin-Walled Structures*, 23, 283-293.
[39] Berry P.A., Rotter J.M. & Bridge R.Q. (2000) "Compression tests on cylinders with axisymmetric weld depressions" *ASCE Journal of Engineering Mechanics*, 126(4), 405-413.
[40] Sadowski A.J. & Rotter J.M. (2011a) "Steel silos with different aspect ratios: I – Behaviour under concentric discharge" *J. of Const. St. Rsrch.*, 67, 1537-1544.
[41] Chen L., Doerich C. & Rotter J.M. (2008) "A study of cylindrical shells under global bending in the elastic-plastic range" *Steel Construction – Design and Research*, 1(1), 59-65.
[42] Gillie M. & Holst J.M.F.G. (2003) "Structural behaviour of silos supported on discrete, eccentric brackets" *Journal of Constructional Steel Research*, 59, 887-910.
[43] Song C.Y., Teng J.G. & Rotter J.M. (2004) "Imperfection sensitivity of thin elastic cylindrical shells subject to partial axial compression" *Int. J. of Sol. & Str.*, 7155-7180.
[44] Sadowski A.J. & Rotter J.M. (2011b) "Steel silos with different aspect ratios: II – Behaviour under eccentric discharge" *J. of Const. St. Rsrch.*, 67, 1545-1553.
[45] Teng J.G. & Song C.Y. (2001) "Numerical models for nonlinear analysis of elastic shells with eigenmode-affine imperfections" *Int. J. Solids & Structures*, 38, 3263-3280.
[46] EN 1993-1-6 (2007) "Eurocode 3: Design of steel structures, Part 1.6: General rules - Strength and stability of shell structures" *Comité Européen de Normalisation*, Brussels.
[47] Dai, K., Huang Y., Gong C., Huang Z., & Ren X. (2015) "Rapid seismic analysis methodology for in-service wind turbine towers" *Earthquake Engineering and Engineering Vibration*, 14:539-548.
[48] Chopra A.K. (2011) "Dynamics of Structures. 4th Ed." *Prentice Hall*, USA.
[49] Mavroeidis G.P. & Papageorgiou A.S. (2003) "A mathematical representation of near-fault ground motions" *Bulletin of the Seismological Society of America*, 93(3), 1099-1131.
[50] Ancheta T.D., Darragh R.B., Stewart J.P., Seyhan E., Silva W.J., Chiou B.S.J., Wooddell K.E., Graves R.W., Kottke A.R., Boore D.M., Kishida T. & Donahue J.L. (2013) "PEER-NGA West2 Database" Pacific Earthquake Eng. Research Centre, Report PEER 2013/03, May 2013
[51] Bommer J.J., Stafford P.J. & Alarcón (2009) "Empirical equations for the prediction of the significant, bracketed and uniform duration of earthquake ground motion" *Bulletin of the Seismological Society of America*, 99(6), 3217-3233.
[52] Luco N. & Cornell C.A. (2007) "Structure-specific scalar intensity measures for near-source and ordinary earthquake ground motions" *Earthquake Spectra*, 23(2), 357-392.
[53] Jalayer F. & Cornell C.A. (2002) "Alternative nonlinear demand estimation methods for probability-based seismic assessments" *Earthquake Engineering and Structural Dynamics*; 38, 951-972.
[54] Cornell C.A., Jalayer F., Hamburger R.O. & Foutch D.A. (2002) "Probabilistic basis for 2000 SAC Federal Emergency Agency steel moment frame guidelines" *ASCE J. Str. Eng.*, 128(4), 526-533.
[55] Camara A., Ruiz-Teran A.M. & Stafford P.J. (2013) "Structural behaviour and design criteria of under-deck cable-stayed bridge subjected to seismic action" *Earthquake Engineering and Structural Dynamics*, 42(6), 891-912.
[56] Camara A. & Astiz M.A. (2014) "Analysis and control of cable-stayed bridges subjected to seismic action" *Structural Engineering International*, 24(1), 27-36.
[57] Hancock J. & Bommer J.J. (2006) "A state-of-knowledge review of the influence of strong-motion duration on structural damage" *Earthquake Spectra*, 22, 827-845.
[58] Elgamal A. & He L. (2004) "Vertical earthquake ground motion records: An overview" *Journal of Earthquake Engineering*, 8(5), 663-697.
[59] Málaga-Chuquitaype C., Elghazouli A.Y. & Bento R. (2009) "Rigid-plastic models for the seismic design and assessment of steel framed structures" *Eqk. Eng. and Str. Dyn.*, 38(14), 1609-1630.